Analytica Chimica Acta 1081 (2019) 146–156

Contents lists available at ScienceDirect

Analytica Chimica Acta

journal homepage: www.elsevier.com/locate/aca

# Aptamer-based SERS biosensor for whole cell analytical detection of *E. coli* O157:H7

Susana Díaz-Amaya [a, *], Li-Kai Lin [a], Amanda J. Deering [b], Lia A. Stanciu [a, c]

[a] Department of Materials Engineering, Purdue University, West Lafayette, IN, 47907, USA
[b] Department of Food Science, Purdue University, West Lafayette, IN, 47907, USA
[c] Birck Nanotechnology Center, Purdue University, West Lafayette, IN, 47907, USA

## GRAPHICAL ABSTRACT

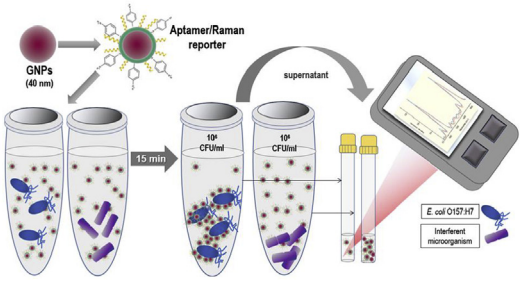


## ARTICLE INFO

*Article history:*
Received 9 May 2019
Received in revised form
26 June 2019
Accepted 15 July 2019
Available online 17 July 2019

*Keywords:*
*Aptamers*
*E. coli O157:H7*
*Food safety*
*Rapid detection*
*SERS nanoprobes*
*Surface enhanced Raman spectroscopy*

## ABSTRACT

Infectious outbreaks caused by foodborne pathogens such as *E. coli* O157:H7 are still imposing a heavy burden for global food safety, causing acute illnesses and significant industrial impact worldwide. Despite the growth of biosensors as a research field, continuous innovation on detection strategies, novel materials and enhanced limits of detection, most of the platforms developed at the laboratory scale never will get to meet the market.

The use of aptamers as capture biomolecules has been proposed as a promising alternative to overcome the harsh environmental conditions of industrial manufacturing processes, and to enhance the performance under real, complex, conditions. In this work, we present the feasibility of using aptameric DNA sequences, covalently conjugated to 4-aminothiophenol-gold nanoparticle complexes for the sensitive and highly specific detection of *E. coli* O157:H7 via surface enhanced Raman spectroscopy (SERS) analysis. Low concentrations of *E. coli* O157:H7 were detected and quantified within 20 min in both pure culture (~$10^1$ CFU mL$^{-1}$) and ground beef samples (~$10^2$ CFU mL$^{-1}$). The SERS intensity response showed a strong negative linear correlation ($r^2 = 0.995$) with increasing concentrations of *E. coli* O157:H7 (ranging from $10^2$ to $10^6$ CFU mL$^{-1}$). High specificity was achieved at genus (*L. monocytogenes, S. aureus S. typhimurium*) species (*E. coli* B1201) and serotype (*E. coli* O55:H7) level, demonstrating with 95% of confidence that the interferent microorganisms tested generated a Raman signal response not significantly different from the background ($p = 0.786$).

This work evaluates the incorporation of aptameric DNA sequences as bio capture molecules exclusively. The successful performance presented using non-modified citrate reduced GNPs, is promising for

* Corresponding author.School of Materials Engineering, Neil Armstrong Hall of Engineering, Purdue University. 701 West Stadium Avenue, West Lafayette, IN, 47907-2045, USA.
*E-mail addresses:* diaz102@purdue.edu (S. Díaz-Amaya), lin688@purdue.edu (L.-K. Lin), adeering@purdue.edu (A.J. Deering), lstanciu@purdue.edu (L.A. Stanciu).

https://doi.org/10.1016/j.aca.2019.07.028

potential low-cost, high-throughput applications. The findings might be applied simultaneously to the detection of a wide variety of foodborne pathogens in a multiplexed fashion employing unique Raman probes and strain-specific aptamer sequences.



## 1. Introduction

Infectious diseases have been historically ranked on top as one of the major challenges for human survival due to the periodical epidemic emergence of old and new outbreaks [1]. Foodborne infections are frequently transmitted by food contamination or cross-contamination during production, processing or transportation. Despite continuous efforts to improve safe-handling and processing practices, outbreaks caused by foodborne pathogens continue to arise, posing an imminent risk that needs to be effectively addressed.

*E. coli* O157:H7 is a well-known multihost pathogen; this sera-variety shows several undesirable characteristics that express together, evolving in one of the most serious health threats. Infections caused by these bacteria can lead to hemolytic uremic syndrome (HUS), characterized by hemolytic anemia, thrombocytopenia, and potential renal injury [2]. *E. coli* O157:H7 is responsible for more than 2 million acute illnesses annually worldwide [3]. According to the Center for Disease and Control Prevention (CDC), the most recent outbreak of Shiga toxin-produced by *E. coli* O157:H7 in the USA led to a balance of more of 210 people reported as sick in 36 states. These numbers unveil the urgent need for rapid, sensitive, and specific high throughput detection strategies within the food production chain, water supply, and distribution systems [4,5]. Traditional methods for the detection of foodborne pathogenic bacteria mainly rely on specific biochemical and molecular (immunological o DNA-based) identification. Conventional plate counting for *E. coli* O157:H7 confirmation in food samples involve enrichment, isolation, and a multi-step detection process that results in a time-consuming procedure (up to 7 days for confirmation) [6,7]. Immunological identification involves highly specific antibody-antigen interactions, with the shortcoming that antibodies are produced in vivo; this represents high costs, complex production processes, limited availability of capture molecules for new targets, poor physical and chemical stability, and significant batch to batch variation [8,9]. Molecular detection is mainly based on genomic or plasmid DNA analysis by polymerase chain reaction (PCR). Despite high sensitivity and specificity, identification via molecular methods requires rigorous sample processing (cell lysis, DNA extraction, purification, and amplification), as well as specialized instrumentation, and trained personnel [7,10,11]. The practical implementation of PCR is commonly restricted to identity confirmation purposes rather than the high throughput real-time screening required for food safety applications.

Spectroscopy tools such as mid-IR, have shown important potential towards the development of simple techniques that require minimal sample preparation, and provide cost-efficient, sensitive fast response and quantitative analysis as an approach to assure global food safety [12]. Raman scattering spectroscopy provides structural and chemical information on molecules based on the specific vibrational shifts that occur when changes in their polarizability are registered upon exposure to IR light [13]. Significant progress in pathogen detection strategies has been made during the last decades thanks to the development of surface enhanced Raman spectroscopy (SERS). The use of SERS is eliminating the need for pathogen culturing by taking advantage of the characteristic surface plasmon resonance of metallic nanoparticles, which act as signal enhancing substrates. Surface bound highly affine capture bio-molecules functionalize these particles to add up a layer of specificity, allowing whole-cell pathogen fingerprinting [14].

Multiple strategies have been proposed for SERS-based detection of *E. coli* O157:H7 using monoclonal antibodies as capture molecules. In one study, the reported detection limits reached were$10^3$ CFU $mL^{-1}$ when antibodies were conjugated on Ag/Au core-shell nanoparticles [15]. In antoher report, the detection limit was pushed to 10 CFU $mL^{-1}$ when additional centrifugal filtration was applied to the bacteria-Raman complexes (Raman reporter-GNPs), followed by a silver intensification step [16]. Additional developments have been achieved with core-shell GNPs with embedded reporter molecules and antibody-conjugated magnetic nanoparticles (MNP) for selective concentration, leading to a LOD of 10 CFU $mL^{-1}$ [17].

Despite all the efforts for the development of detection technologies, most lab-scale devices never get to meet the market [18]. This is mainly due to the lack of repeatability once the sample size is increased (high scale), prohibitively high costs of manufacturing, poor stability of biomolecules and the use of sophisticated instrumentation that poses a restriction in terms of costs and high-throughput. Therefore, the evident disconnection between early design & development stages and industrial level manufacturing is posing one of the major challenges to overcome the problem represented by infections.

The rapid emergence of aptamers as alternative capture molecules, with high specificity and environmental robustenss has opened up the discussion on a potential new generation of diagnostic platforms, more amenable to industrial manufacturing. Aptamers are single-strand DNA/RNA sequences that can detect potentially any target with high specificity. Other advantages of aptamers compared to antibodies are small size, chemical synthesis, low cost, high stability, batch to batch reproducibility and no-restrictions regarding target size or immune response. In line with the potential advantages of incorporating aptamers as superior capture biomolecules, their performance has been explored as a novel strategy for the fabrication of next-generation biosensing devices. Various reports demonstrate the aptameric ability to capture with high affinity a wide range of targets going from small ions such as Mercury ($Hg^{2+}$) [19] to whole cell bacteria [20,21]. To date, a number of strategies have been described for the effective aptamer-based detection of *E.coli* O157:H7. These include colorimetric spectroscopy, where taking advantage of the immobilization of a specific aptamer on the surface of nanoscale polydiacetylene (PDA) vesicles led to an optical LOD in fecal samples of $10^8$ CFU $mL^{-1}$ [22]. Another example is an optical lateral flow assay (LFA) applying aptamer-mediated strand displacement amplification that pushed the LOD down to 100 CFU $mL^{-1}$ in non-complex food matrices such as milk and apple juice [23]. More recently, a quartz crystal microbalance aptasensor (QCM) with a LOD of $10^3$ CFU $mL^{-1}$ in PBS was reported [21].

Despite the potential of aptamer-mediated strand displacement LFA, this method relies on DNA amplification rather than whole cell detection, adding a complexity layer to the detection mechanism by imposing a rigorous sample preparation. In addition, considering

the "zero tolerance" policy ruled by USDA, there is still an urgent need to develop novel strategies that might take the portable on-site biosensing technologies near to regulatory compliance with demonstrated efficiency not only in non-complex samples such as milk or juice, but also in complex samples, such as ground beef.

With the emergence of portable hand-held IR spectrometers, the potential implementation of SERS-based strategies for rapid, real-time, and on-site monitoring of pathogenic and toxic agents became of great interest. Along these lines, the rapid development of SERS-based technologies coupled with aptameric capture biomolecules for pathogen detection holds significant interest and potential.

SERS technologies combined with aptameric detection were succesfully reported for *Salmonella typhi* (LOD of $10^2$ CFU mL$^{-1}$) [15], *S. aureus* (LOD of 10 CFU mL$^{-1}$) [24], and *S. typhimurium* (15 CFU mL$^{-1}$) [25]. Recently, Zhang and collaborators presented a novel approach for dual recognition of *E.coli* and *S. aureus* using vancomycin-modified $Fe_3O_4$@Au magnetic nanoparticles ($Fe_3O_4$@Au-Van MNPs) with a LOD of 50 CFUmL$^{-1}$ [26]. Despite promising results, this work describes the application of an aptameric sequence affine for a non-pathogenic *E. coli* strain. This conclusion is drawn from the results presented for capture efficiency, where the colonies of *E. coli* are grown in blood agar showing no signs of hemolysis. From literature, the enterohemolytic phenotype is typical of the human pathogenic Shiga-toxin producer E. *coli* (STEC) strains, such as *E. coli* O157:H7 [27,28]. For the on-site implementation of novel and efficient pathogen detection techniques, it is mandatory to guarantee the specific detection of pathogenic targets, avoiding any possibility of false negatives. Therefore, the use of aptamers for rapid and reliable detection of human Shiga-toxin producer pathogens is still growing as a topic of great scientific interest.

Despite an increasing number of new detection platforms incorporating aptamers, there is no aptamer-based SERS platform for the detection of the pathogenic Shiga-toxin producer strain *E. coli* O157:H7 reported to date. This work aims to demonstrate the feasibility of using, for the first time, a truncated aptameric DNA sequence highly specific for *E. coli* O157:H7, covalently conjugated to 4-aminothiophenol-gold nanoparticles as capture biomolecules for the sensitive and highly specific detection of *E. coli* O157:H7 by SERS analysis. To the best of our knowledge, this is the first reported aptamer based-SERS whole cell detection of Shiga-toxin producer *E. coli* O157:H7 in real food samples.

## 2. Experimental

### 2.1. Materials

Citrate-capped GNPs (40 nm) were synthesized by Nanopartz Inc. (Loveland, CO, US). Thiol-functionalized aptamers for *E. coli* O157:H7 [20] were synthesized by Integrated DNA Technologies (Skokie, IL, US), 4-aminothiophenol (97%) was from Sigma Aldrich Co. (St. Louis, MO, US), and ethanolic solutions were prepared using Ethanol 190 proof (95%) USP, Decon labs (King of Prussia, PA, US). All glassware was from VWR Intl. (Batavia, IL, US). It was cleaned with aqua regia HCl: HNO3 (3:1) and washed with deionized water before use. Phosphate Buffer Solutions (PBS) used in this work were liquid, sterile-filtered, suitable for cell culture, from Sigma Aldrich Co. (St. Louis, MO, US) (10 mM, pH 7.4). Raman Spectroscopy sample tubes were purchased from New Era Enterprises (Vineland, NJ, US).

### 2.2. Instruments

Bright-field transmission electron microscopy (TEM) images of the GNPs, Raman complex (4-ATP-GNP) and Raman complex-bacteria conjugates were acquired using a Tecnai G2 20 TEM (ACC V: 200 kV) (FEI Corp., Hillsboro, OR, US). GNP and Raman complex zeta potential data were obtained using a Zetasizer Nano Z (Malvern Instruments Ltd., Westborough, MA, US). Optical densities were measured using a SpectraMax Plus 384 (Molecular Devices, L.L.C., Sunnyvale, CA, US). Raman spectra were acquired using a Complementary FT-Raman capability for Nicolet 6700 FT-IR spectrometer (Thermo Scientific Co. Grand Island, NY).

### 2.3. Microorganisms

*E. coli* O157:H7, *Listeria monocytogenes*, *Staphylococcus aureus*, *E. coli* B1201, *E. coli* O55:H7 and *Salmonella Typhimurium* strains were available from the Food Science Department-Purdue University. Fresh cultures were first plated in LB agar (Thermo Fisher Scientific, Waltham, MA), allowing overnight growth. A single colony of each microorganism was transferred to sterile LB broth and cultured in a temperature controlled orbital shaker (MaxQ™ HP Incubated Tabletop) at 35 °C and 160 rpm for 24 h. Cell enumeration of *E. coli* O157:H7, *E. coli* B1201, *E. coli* O55:H7, *Listeria monocytogenes*, *Staphylococcus aureus*, and *Salmonella Typhimurium* were conducted with the traditional viable plate count method by preparing serial dilutions in PBS (pH 7.4) and spreading 100 μl of each diluted sample on the specific media surface (using glass spreaders) [29]. Specific energy sources were used for specific and/or selective growth of *E. coli* O157:H7, *E. coli* B1201, *E. coli* O55:H7 in MacConkey agar with sorbitol (SMAC), modified Oxford agar (MOX), Brain Heart Infusion Agar (BHI), and Xylose Lysine Tergitol-4 agar (XLT-4) (BD Difco, Franklin Lakes, NJ) respectively. Plates were incubated at 35 °C for 48 h; the stock concentration was calculated by serial dilutions and plate counting from plates containing between 30 and 300 colony forming units (CFU).

### 2.4. Preliminary affinity test (electrophoresis)

The DNA sequences used for the electrophoretic test were first reported by Bruno JG, and Chanpong J [30], who presented a proprietary method for aptamer selection based on the ability of these sequences to bind with high specificity to lipopolysaccharides (LPS) of the *E. coli* O157:H7 membrane. Later on, Wu and collaborators demonstrated the promising performance of these sequences by modifying the truncated LPS-binding aptamer on the surface of nanoscale polydiacetylene (PDA) vesicles achieving an optical LOD of $10^8$ CFU mL$^{-1}$ in real complex samples [22]. Recent results presented by Wei and collaborators demonstrated their efficiency for whole cell capture of *E. coli* O157:H7 by incorporating both sequences as capture biomolecules in an aptamer-based lateral flow assay pushing the LOD down to 100 CFU mL$^{-1}$ in non-complex matrices such as milk and apple juice [23].

The sequences are identified as a-aptamer [5′ATCAAATGTGCAGATATCAAGACGATTTGTACAAGATCCATGCTGAGGTGGTCATAGCTGATCCTACC], and c-aptamer [5′TTTCCGGACGCTTATGCCTTGCCATCTACAGAGCAGGTGTGACGG]. Both aptameric sequences were heat annealed (90 °C/2 min) and allowed to slowly cool down in order to provide optimal folding. Liquid bacterial cultures of *E. coli* O157:H7, *S. typhi,* and *L. monocytogenes* were purified by washing (5000 rpm/2 min) and resuspended in PBS (pH 7.4). The aptameric solution (10 μM in nuclease-free water) was incubated with pure bacterial suspensions (PBS pH 7.4) at a ratio of 10:1 (v/v) for each experiment. After 30 min of incubation at room temperature under orbital agitation (100 rpm), any excess of aptamer was removed by a final washing step (5000 rpm/2min) and resuspension in 20 μl of PBS. The samples were labeled with GelRed (Biotium, Fremont, CA, US), and loaded into a polymerized agarose gel (4 wt%). A horizontal Mini-Sub® Cell GT electrophoresis chamber (Bio-Rad, Hercules, CA,

US) was used to run the samples by applying an electric field of 110 mV for 40 min. Finally, the bands were visualized using a Gel Doc™ XR + Gel Documentation System (Bio-Rad, Hercules, CA, US) by UV-transillumination. Finally, the prediction of secondary structures (folding) of both aptameric sequences was obtained using RNA structures software package, available for free download at http://rna.urmc.rochester.edu/RNAstructure.html.

### 2.5. Assembly of AuNPs-Raman reporter complexes

#### 2.5.1. Surface modification (Raman reporter)

GNPs surfaces were modified with 4-aminothiophenol (4-ATP) at molar ratio 4-ATP: Au 15:1, 18:1 and 34:1 in ethanolic solution. The mix was then stirred for 2 h and kept at 4 °C for 12 h [31]. The subsequent washing step was performed by centrifugation (1,4 RCF for 15 min) to remove the excess of 4-ATP.

#### 2.5.2. Thiol-aptamer-AuNPs functionalization

Based on the preliminary affinity test, the a-aptamer was used for the fabrication of Raman reporter complexes. The DNA sequence was modified with a thiol functionalization (IDT Integrated DNA technologies). (a-aptamer) [5′Thiol/ATCAAATGTGCAGATATCAA GACGATTTGTACAAGATCCATGCTGAGGTGGTCATAGCTGATCCTACC]. Next, the thiol groups were chemically activated by disulfide bond reduction using Tris(2-carboxyethyl) phosphine hydrochloride, TCEP with a molar excess (DNA: TCEP) of 1:10 (Thermo Fisher Scientific, Waltham, MA). The DNA aptameric sequence was functionalized with the 4-ATP-GNPs at a molar ratio of 100:1 according to the method previously reported [31]. Bovine serum albumin, BSA (10% PKL, Seracare) was added in a ratio 1:10 (v/v), to block any unbound amine group, the mix was incubated for 30 min, and washed by a final centrifugation step. Blocked Raman reporter complexes (aptamer-4-ATP-GNPs) were concentrated ten times and re-suspended in PBS (pH 7.4).

### 2.6. Raman spectra acquisition

#### 2.6.1. Data acquisition from pure culture

Each tested bacterial strain was serially diluted in PBS (pH 7.4) reaching concentrations ranging from $10^1$ to $10^6$ CFU $mL^{-1}$. Then, 200 μl of the aptamer-Raman complex was mixed with 100 μl of bacteria culture and incubated at room temperature for 15 min. After incubation time, the mix was loaded in Raman Spectroscopy sample tubes for spectroscopic analysis. Raman spectra were collected using a Thermo Nicolet 6700 FT-IR/FT Raman spectrometer (Thermo Scientific Co. Grand Island, NY). The excitation laser source was provided by 1064 nm at resolution 8 in the 100-4500 $cm^{-1}$ range.

#### 2.6.2. Data acquisition from ground beef

Standard sample preparation was followed. Ground beef (1 g) was homogenized in 10 mL of sterile PBS (pH 7.4), spiked with *E. coli* O157:H7 suspensions until concentrations of $10^2$ and $10^3$ CFU $mL^{-1}$ were reached. Then the samples were loaded into a sterile stomacher bag (400 mL, Gosselin ™ Sterile Polyethylene Blender Bags) and the mix was homogenized by the stomacher 400 circulator (Seward Ltd., England) for 30 s. Each sample was subjected to the exact same procedure described in the above section (2.5.1).

### 2.7. Data analysis

The analysis of the spectra obtained, and their correlation was made in Origin 2018. Statistical analysis was conducted by One-way ANOVA test, accompanied by Means comparison using Dunnett's method (statistical package JMP).

## 3. Results and discussion

### 3.1. Aptamer-target: preliminary specificity test

To develop sensitive and highly specific SERS probes for the detection of *E. coli* O157:H7, it was key to evaluate the binding affinity of the candidate aptamers for the target bacteria. As a preliminary specificity test, two aptameric sequences (a-aptamer and c-aptamer) [23] were incubated with purified bacterial suspensions (*E. coli* O157:H7, *S. typhi* and *L. monocytogenes)* in independent experiments under the same conditions. Specific interactions were evaluated by taking advantage of the small pore size of agarose at high concentration (4%), and the mobility and diffusion of DNA under electrical field. The characteristic separation of nucleic acids bands as a function of molecular weight in electrophoretic experiments made possible the visible identification of free (unbonded) DNA strands with a band size around 80 base pairs (bp) and high weight bands for the strands interacting with the bacterial cells.

Fig. 1(a) shows the enhanced image of the agarose gel after electrophoresis and UV-transillumination. *E. coli* O157:H7 cells were incubated with both aptamers (c-aptamer & a-aptamer, 10 μM) and the results are visible in lanes (1) and (4), respectively. The bands reveal that both aptameric sequences are able to capture the target. Therefore, the aptamers follow a conformational change (secondary structure) as illustrated in Fig. 1(b) and **(c),** restricting the mobility of DNA through the gel matrix. The secondary structure prediction of the aptamers tested was obtained by SHAPE mapping data, using then Rsample algorithm described by Spasic and coworkers, which relies on the thermodynamic nearest neighbor model for RNA/DNA folding [32]. Despite the demonstrated binding affinity observed by both aptameric sequences tested, lane (1) shows an additional band corresponding to a secondary interaction of the c-aptamer with an extracellular compound of high molecular weight (~1000 base pairs) acting as a secondary binding site. It has been reported that *E. coli* O157:H7 and *E. coli* O104:H4 share more than 137 extracellular proteins [23] and *E. coli* O157:H7, like many other pathogenic *E. coli* strains, use type II extracellular secretory systems, which are conserved in other non-pathogenic strains [24]. This could easily lead to false positives. On the other hand, lane (4) shows a clean single band, where the a-aptamer is completely retained by its highly affine interaction with LPS of the outer surface bacterial membrane. The described results make of this sequence an optimal candidate for the specific whole cell detection approach. Lanes (2) and (3) show the results from pure cell samples of *S. typhi* and *L. monocytogenes* respectively, demonstrating that there is not any genetic material released (as evidence of cell integrity) during testing. Lanes (5) and (6), show the interaction of a-aptamer *with S. typhi* and *L. monocytogenes*. Since there is no binding site on the surface of those bacteria cells, the DNA conserves its linear conformation and moves freely, diffusing through the gel and reaching a band size that is in complete agreement with the initial size showed by the sole DNA a-aptamer (~80 bp, lane 7). These results confirm the specific affinity interaction between the aptameric sequence (a-aptamer) and *E. coli* O157:H7 as whole cell target. The results demonstrate that both aptamers tested present no interaction with other potentially interfering bacteria surfaces, and thus the binding is specific to *E. coli* O157:H7. Since the a-aptamer exhibited better performance, this sequence was selected for further experiments.

### 3.2. Raman probe optimization

To maximize signal response, the fabrication process followed a layer-by-layer optimization. First, the label molecule 4-aminothiophenol (4-ATP) was assembled on the GNPs surface at

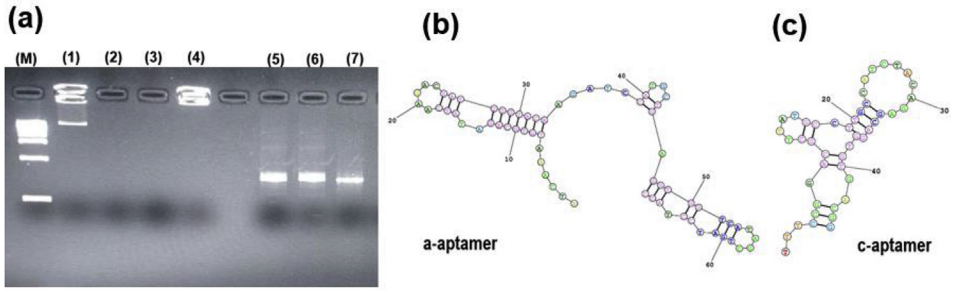


**Fig. 1.** Aptamer-target preliminary test: electrophoresis agarose gel showing the interaction between 2 aptamers specific for *E. coli* O157:H7, and two interferant bacteria strains (a): molecular marker (M), c-aptamer-*E. coli* O157:H7 (1), *Salmonella typhi* (2), *L. monocytogenes* (3), a-aptamer-*E. coli* O157:H7 (4) a-aptamer- *Salmonella typhi* (5), a-aptamer-*L. monocytogenes* (6) and a-aptamer (7); DNA secondary structure predictions of a-aptamer (b) and c-aptamer (c) obtained by SHAPE mapping data.

increasing concentrations ranging from 30 to 100 mM, and the reporter performance was assessed by Raman Spectroscopy Fig. 2 **(a)**. A plot that highlights the difference in Raman intensities at different 4-ATP concentrations is presented in Fig. 2 **(b).** SERS signal enhancement is controlled by the GNPs surface area, particle shape, and the availability of binding sites. According to previous reports, the size of GNPs presents a positive and direct correlation with 4-ATP-SERS signal enhancement, and reaches a critical point near 50 nm. As particle size increases, the SPR moves closer to the excitation wavelength of the laser until reaching the critical size. After critical size, it moves away from the vibrational mode, therefore the enhancement decreases [25]. Thus, the GNPs size was set at 40 nm to maximize SERS enhancement. Collected spectra show both peaks characteristic for 4-ATP at 1078 $cm^{-1}$ and 1590 $cm^{-1}$, corresponding to the stretching vibrations of C–S and C–C, respectively. Due to its higher intensity, the peak at 1078 $cm^{-1}$ was used to compare the intensity of the different Raman probes tested.

Results in Fig. 2 **(a)(b)** showed an increase in the Raman intensity signal for concentrations 30 mM, 40 mM, and 50 mM, with significant differences among them ($p < 0.05$). For the last concentration tested (100 mM), the collected spectrum shows a very slight increase in the Raman intensity, which is not significantly different from the one obtained with 50 mM ($p = 0.71$), serving as

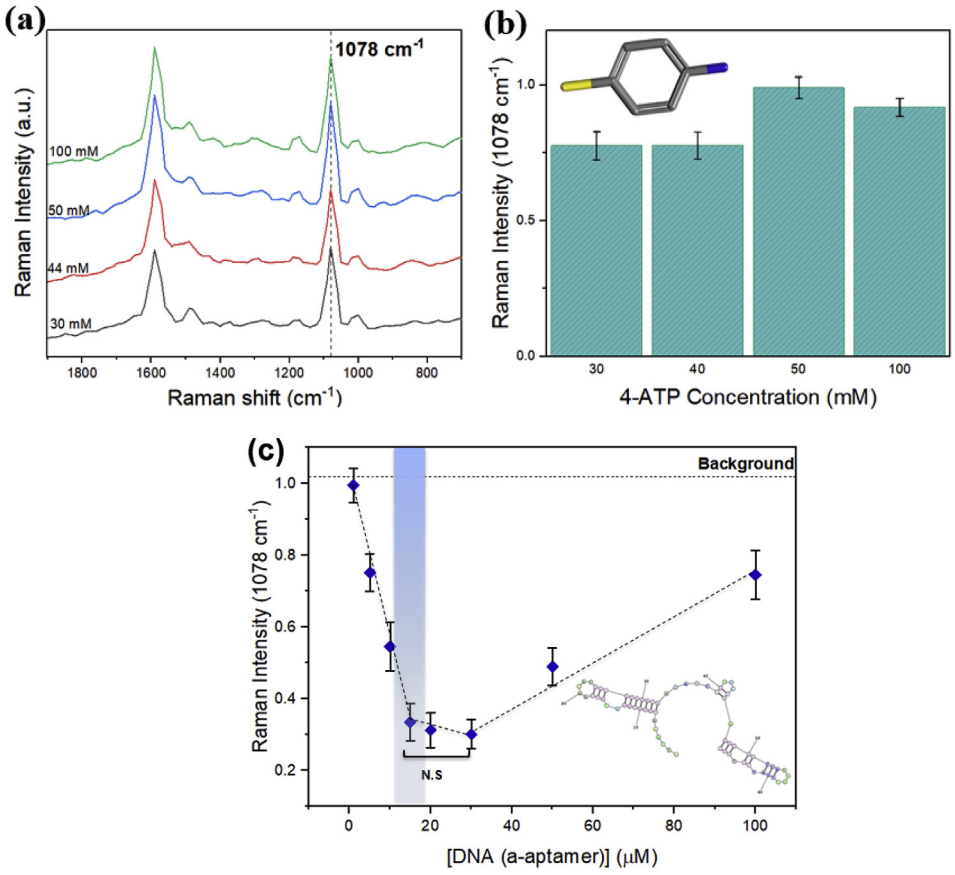


**Fig. 2.** Optimization of enhanced intensity (4-ATP- GNPs): Raman spectra of increasing concentrations of ATP (ranging from 30 to 100 mM) (a); maximum intensities at 1078 $cm^{-1}$ under increasing concentrations of 4-ATP (b). Aptamer coverage optimization (aptamer-4-ATP-GNPs): Raman intensity response with a fixed coating of 4-ATP (50 mM), under increasing concentrations of a-aptamer (5–100 μM). The intensity of the response was evaluated by testing a known concentration of *E. coli* O157:H7 ($10^4$ CFU $mL^{-1}$) The results presented correspond to the average response of at least 3 independent measurements. The error bars show the standard deviation from the mean value.

evidence of the saturation of the GNP surface. For further experiments, the critical concentration of 4-ATP was set at 50 mM.

After analysis of the best coverage for the label layer (4-ATP), a thiol-DNA layer was optimized by comparing the SERS response (1078 $cm^{-1}$) of the as-fabricated Raman reporters under increasing concentrations of a-aptamer (ranging from 5 to 100 μM). The thiol-DNA was immobilized as a self-assembled layer on unoccupied sites of gold by thiol-Au bonding. After incubation with a fixed concentration of *E. coli* O157:H7 ($10^4$ CFU $mL^{-1}$), all samples were treated by using the protocol described in the experimental section (2.6.1). According to the results (Fig. 2(c)), increasing concentrations of a-aptamer (from 5 to 15 μM) resulted in an inversely proportional effect on the SERS signal, which relates with an increased probability of successful binding events. These results agree with the detection mechanism proposed, i.e. the signal response is generated from the unbound Raman probes that are collected from the supernatant after the binding event. However, when the concentration of aptamer was further increased (15–30 μM), the SERS signal intensity reached a plateau ($p = 0.152$). Finally, when the concentration was even further increased up to 100 μM, the SERS signal increased, indicating a reduction of the capture ability. The extent to which an increased density of the capture biomolecules leads to SERS signal suppression has been explained by the crowding effect and steric hindrance [33]. The immobilized aptamers must overcome the packing limitation to perform a secondary conformational change and achieve a successful interaction with the target. Therefore, increasing the aptamer concentration beyond a certain point, will result in signal suppression [34]. Thus, based on the results displayed in Fig. 2(c), the optimum DNA-a-aptamer concentration was set to 15 μM.

### 3.3. Materials characterization

4-aminothiophenol (4-ATP) was self-assembled on the surface of gold nanoparticles (GNPs), followed by the conjugation of the thiol-modified DNA sequence (a-aptamer) by stable interactions provided by thiol-gold bonds on any unoccupied site of the GNPs surface. The enhancing substrate (GNPs) was characterized during the assembling process by UV–vis spectroscopy, ζ potential measurements, and TEM imaging. According to the results shown in Fig. 3 **(a)**, the surface plasmon resonance (SPR) of the 40 nm citrate reduced GNPs presented an absorption peak within the visible spectrum with a $\lambda_{max}$ of 520 nm. As a function of the number of layers added, the absorption peak redshifted as a confirmation of the self-assembled layers on top of the enhancing substrate. Assembling of 4-ATP resulted in a redshift with a $\lambda_{max}$ of 530 nm. The bonding of the aptameric sequence by thiol-Au bond was confirmed by a slight redshift to $\lambda_{max}$ 534 nm. The UV–vis results are in agreement with the fabrication process proposed (Fig. 3(b)). TEM images of the citrate reduced GNPs served as initial confirmation of the particle size (40 nm) and spherical shape. Microstructure was analyzed as confirmation of a visible monolayer present on the GNPs surface while conserving an undisturbed spherical shape (Fig. 3(d)). Additional metric from ζ potential measurements provided extended information regarding the surface modification by changing the apparent surface potential from −32.4 mV ( ±6.09 mV) for citrate reduced GNPs to −17.9 mV ( ±5.15 mV) for as-fabricated Raman reporter complexes (aptamer-4-ATP-GNPs).

### 3.4. Detection mechanism

Form the light of literature, the use of aptameric sequences as specific capture agents might represent a promising approach for the successful upscaling of biosensors towards industrial production and on-site detection. Aptamers offer special features such as their small size (increased surface coverage), flexible structure (enhanced penetration), ability to recognize small molecules lacking immune response, almost no batch-to-batch variation, high specificity, slow off-rates, and high stability [35,36].

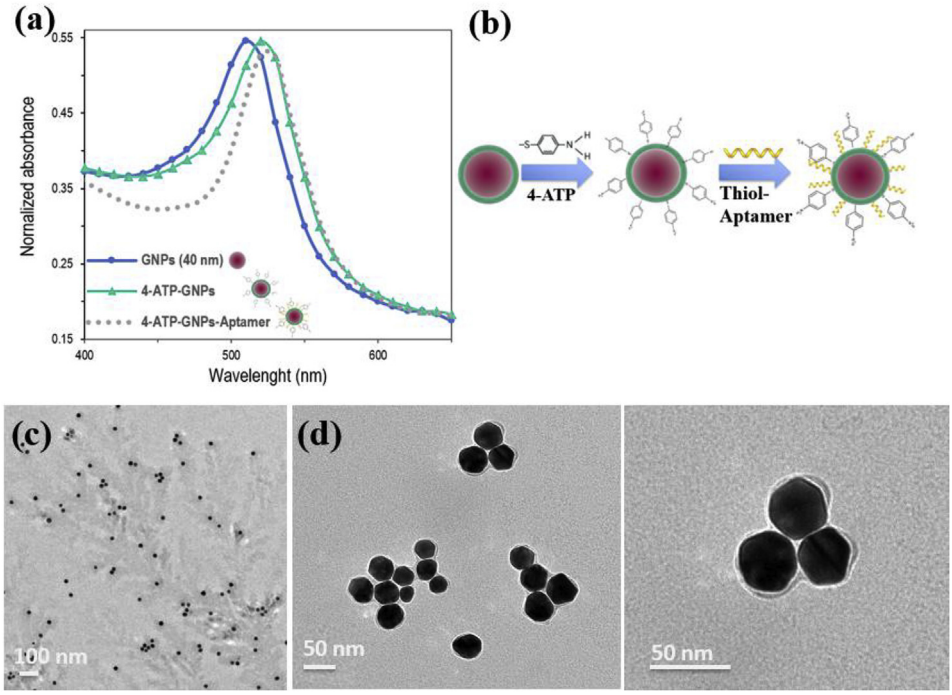


**Fig. 3.** Normalized UV–vis absorption spectra of GNPs, thiol-aptamer-GNPs, and functionalized 4-ATP-aptamer-GNPs complex (a) Bright Field TEM images of 40 nm citrate GNP (b) and 4-ATP-GNPs (c).

The advantages of incorporating aptamers for on-site detection strategies are well described by literature and might represent a potential approach to overcome the limitations of stability and manufacturability of antibodies. Here, we present a simple, rapid and efficient process for whole-cell SERS detection of *E. coli* O157:H7. According to the illustration presented in Scheme 1, known concentrations of *E. coli* O157:H7 cells were incubated at room temperature for 15 min with Raman probes (aptamer-4-ATP-GNPs), resulting in selective bacteria surface decoration by these highly specific complexes.

In a study on the specific interaction of the named a-aptamer and the target cell membrane, Bruno J.G proved the feasibility of aptameric binding to a relatively common epitope on LPS, which might vary in amount per cell, or composition among strains [37]. The whole LPS immobilization on magnetic beads used for SELEX, following screening against whole Big 7 *E.coli* cells, which was targeting O antigens of LPS and core-or fatty acids, led to the enhanced specificity of this aptamer [38].

As an effect of the target size and density, along with the potential electrostatic interactions with surrounding complex agglomerates coming from the food matrix, the Raman probe-bacteria conjugates tend to precipitate with time, leading to cell sedimentation and the consequent generation of a superficial phase where unbounded Raman probes will temporarily reside. The sedimentation was visible by the naked eye after completion of the incubation time when high concentrations ($10^5$ and $10^6$ CFU mL $^{-1}$) of bacteria were tested. Hence, small aliquots (final volume 100 μl) were carefully recovered from the supernatant with a micropipette for further testing.

The chemical potential introduced by the complexity of the matrix tested, and the ionic strength of the diluent media, served as a trigger of the interparticle distance reduction among the unbound Raman probes by shrinking the electrostatic double layer on the GNPs. However, the SPR of the unbound Raman probes was not affected. This stability effect is explained by the electrostatic repulsion from the firmly fixed layer of 4-ATP activating the formation of so called “hot spots” where the SERS signal is obtained. Therefore, increasing concentrations of *E. coli* O157:H7 that are captured leads to a reduction of the number of Raman probes suspended in liquid media, causing a decrease in the SERS signal.

### 3.5. Limit of detection

To assess the detection performance of the fabricated platform, *E. coli* O157:H7 was incubated at different concentrations ranging from $10^1$ CFU mL$^{-1}$ to $10^6$ CFU mL$^{-1}$ with as-fabricated Raman reporter complexes to test for sensitivity. The SERS signal was analyzed by comparing the peak intensity at 1078 cm$^{-1}$ since this wavelength corresponds to one of the typical stretching vibrational peaks of 4-ATP. Fig. 4 **(a)** presents the SERS detection results. The spectra collected revealed a slight decrease in the Raman intensity when testing samples of low concentration ($10^1$ CFU mL$^{-1}$); however, a clear drop in Raman intensity signals resulted from bacteria concentrations ranging from $10^2$ to $10^6$ CFU mL$^{-1}$, compared with the negative control solution (0 CFU mL$^{-1}$). Cellular suspensions are non-homogeneous samples. Hence, the probability that a collection of cells will be perfectly distributed within the solution is very low [27]. When working with concentrations as low as 10 CFU mL$^{-1}$ and volumes as small as a few microliters, some aliquots will contain more than one cell, and others no cells, increasing the chance of retrieving false signals. Despite the apparent difference between the data collected from *E. coli* O157:H7 at a concentration of 10 CFU mL$^{-1}$ (Fig. 4 **(b)**), showing a Raman intensity (0.862±0.099) below the signal for the blank solution (0 CFU mL$^{-1}$; 0.933± 0.06), there is no significant difference between the two signals ($p = 0.173$).

When increasing the cell concentrations from $10^2$ to $10^6$ CFU mL$^{-1}$, the SERS signal intensity drops, which is in line with the expected detection mechanism, where the signal is collected from the Raman probes unbound and suspended in the liquid media. Fig. 4(c) ‘zooms-in’ the SERS detection results for *E. coli* O157:H7 from $10^2$ to $10^6$ CFU mL$^{-1}$. This tendency was observed during all the measurements and the statistical analysis demonstrated that each concentration tested within this range is significantly different from the blank solution ($p < 0.001$). These results confirmed the success of the aptamer-based SERS detection platform with a LOD of $10^2$ CFU/mL$^{-1}$ in pure culture.

### 3.6. Analytical performance

A linear correlation plot was calculated by fitting the mean SERS

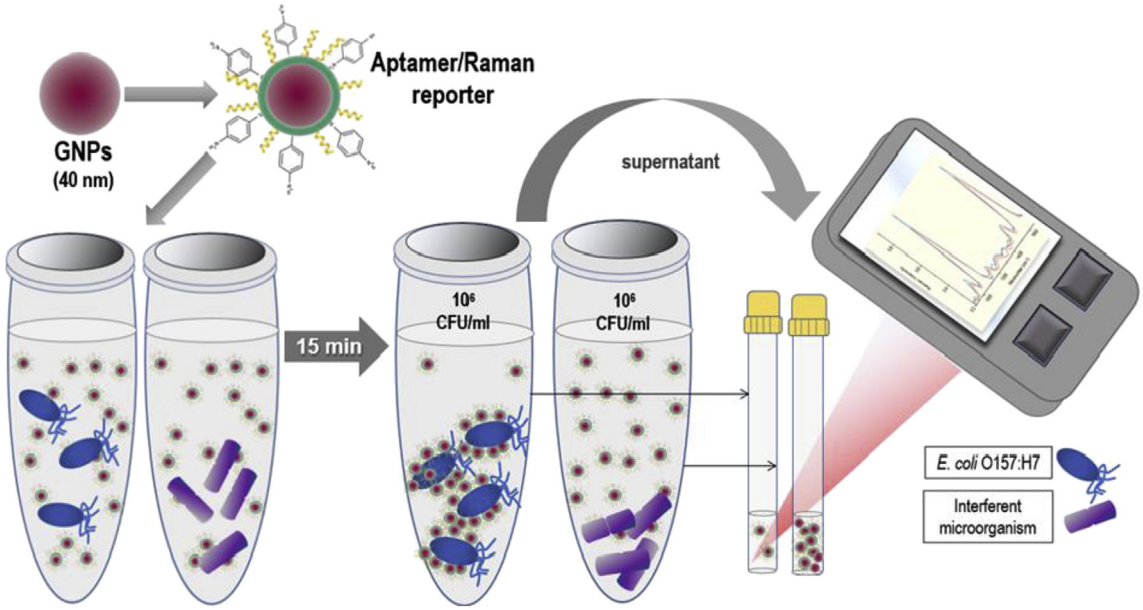


**Scheme 1.** Schematic illustration of the detection mechanism proposed for aptamer-based whole cell detection of *E. coli* O157:H7.

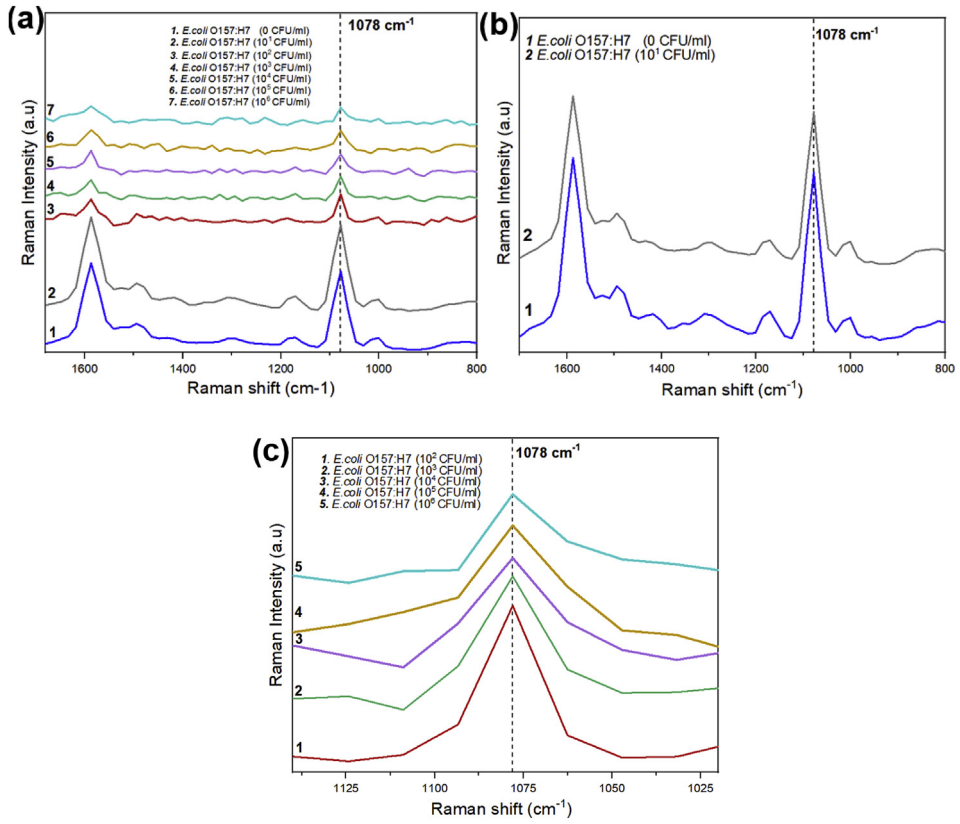


**Fig. 4.** Aptamer-based Surface Enhanced Raman Scattering (SERS). Detection of increasing concentrations of *E. coli* O157:H7 ($10^1$–$10^6$ CFU mL$^{-1}$) (a); detection of $10^1$ CFU mL$^{-1}$ (b) and zoom-in: detection of $10^2$–$10^6$ CFU mL$^{-1}$ (c). All the spectra represent the average of at least 3 independent measurements.

intensity obtained at 1078 cm$^{-1}$ for each tested bacterial concentration tested ($10^2$–$10^6$ CFU mL$^{-1}$). The linear fit presented in Fig. 5 **(a)** shows a negative correlation between SERS intensity and cell concentration, which is consistent with the linear Eq. $Y = -0.0014X+0.394$ ($r^2 = 0.995$). According to the results, the effective limit of detection for the fabricated platform is $10^2$ CFU mL$^{-1}$. TEM images (Fig. 5 **(b) and (c))** revealed a "coating effect" of the Raman probes on the bacterial cell surface (b), and the electrostatic stabilization of unbound Raman probes, where the SERS signal is enhanced(c).

### 3.7. *E. coli O157:H7 detection in real samples*

The reliability of the first aptamer-based SERS platform for detection of *E. coli* O157:H7, was tested by recovery experiments using ground beef (90% lean 10% fat content) as a complex food matrix. This matrix was selected considering its complexity and the fact that most of the infectious cases attributed to *E.coli* O157:H7 worldwide have been linked to raw ground beef. To reduce the interference (noise) attributed to big agglomerates present in complex samples, blender bags with lateral filter were used for homogenization. Samples were spiked with a known concentration of *E. coli* O157:H7, reaching final values of $10^2$ and $10^3$ CFU mL$^{-1}$ in triplicate experiments. Control experiments were run using ground beef homogenized in PBS, and these results are referenced as 0 CFU mL$^{-1}$. All samples were tested under the same conditions, sampling 100 μl of the supernatant after incubation.

Fig. 6(a) presents the spectrum collected after incubation and demonstrate a clear decrease in the Raman intensity at low concentrations of *E. coli* O157:H7 ($10^2$ and $10^3$ CFU mL$^{-1}$), compared with the control samples (0 CFU mL$^{-1}$). This result is in line with the described detection mechanism, where the specific interaction of the aptamer-SERS probes and *E. coli* O157:H7 surface cells, resulted in the reduction of SERS probes suspended, showing a dramatic decrease in the Raman Intensity. The intensity response of all tested concentrations are also in line with the detection mechanism proposed. However, there is a decrease in the signal response (Raman intensity) when testing real samples. This is attributed to the presence of interferent molecules due to the nature of the food matrix, which increases the noise to signal ratio. Statistical analysis by means comparison ($n = 3$) offered evidence that the signal collected from the concentrations tested is significantly different from the control sample ($p < 0.001$).

Table 1 summarizes the recovery performance of the fabricated platform when compared with the initial spiked concentration. For both recovery performance and platform validation, the experimental design accounted for the possibility of having natural contamination in the food matrix by testing an unspiked concentration as a negative control. The recovery efficiency achieved values between 99% and 113% ($n = 3$), with a relative standard deviation (RSD) between 3.65 and 2.89% which represents a promising repeatable approach. In addition, Fig. 6 **(b)** validates the performance of the Aptamer-based SERS platform versus the conventional plate counting method. The results obtained provide evidence of the feasibility to implement the fabricated aptamer-SERS platform for detection of concentrations as low as $10^2$ CFU mL$^{-1}$ in complex matrices for a rapid, on-site, and high-throughput preliminary screening of food samples.

Finally, we demonstrated for the first time, the potential use of aptamers as capture biomolecules for the effective recovery and quantification of *E. coli* O157:H7 in real complex food samples (ground beef), reporting high detection sensitivity, with a limit of

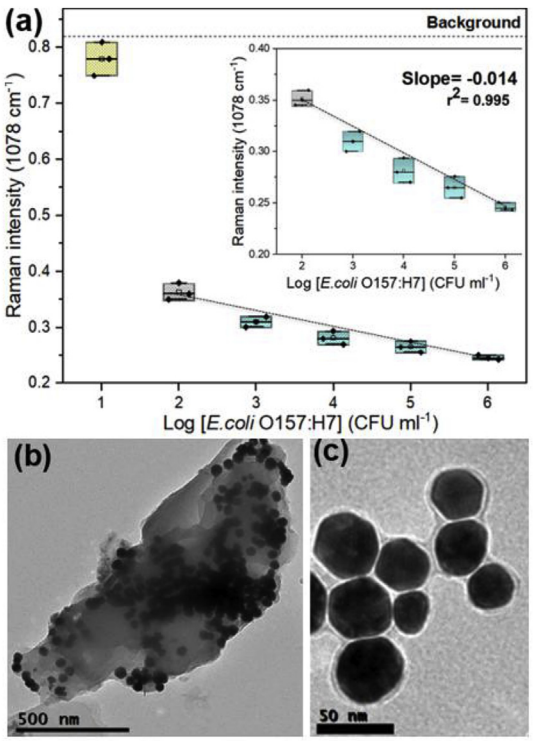


**Fig. 5.** A linear relationship between the Raman intensity and the concentration of *E. coli* O157:H7 on a logarithmic scale. The area of the box represents 1SD, and the error bars 1.5 SD from the mean value (a). Bright field TEM images showing the coating effect of 4-ATP-GNPs on the bacteria surface (b) SERS 'hot-spot' stabilized by electrostatic forces (c).

detection of $10^2$ CFU mL$^{-1}$. Table 2 compares analytical SERS-based platforms reported for detection of *E. coli* O157:H7. Previous approaches which achieved lower LODs than reported herein relied on immune-capture detection, and the samples tested were low in complexity, such as artificially spiked buffer solutions or water samples.

### 3.8. Specificity test

To confirm the high specificity of the aptamer as capture molecule for *E. coli* O157:H7, additional experiments were carried out with an interferent bacteria pool (*E. coli* B1201, *E. coli* O55:H7, *L. monocytogenes, S. aureus,* and *S. thyphi*). High concentrations of all tested microorganisms were selected ($10^6$ CFU mL$^{-1}$), along with blank solutions (0 CFU mL$^{-1}$) accounting for the background. After spectra collection, the Raman intensity responses at 1078 cm$^{-1}$ were calculated for all tested samples (Fig. 7 **(a)).** All samples (*E. coli* B1201, *E. coli* O55:H7, *L. monocytogenes, S.aureus,* and *S. typhi)*, show a Raman spectrum with intensity values in the same range as the negative control sample (no bacteria). Statistical analysis (mean comparison) revealed that there is no significant difference among signals ($p = 0.786$), and the intensity is significantly different ($p < 0.00001$) from the signal obtained by the target (*E. coli* O157:H7) under the same conditions ($10^6$ CFU mL$^{-1}$). These results further confirm the lack of interaction between the Raman probes and the cell surfaces of possible interferent bacterial cells, and are in full agreement with a recent publication that demonstrated the high specificity of this aptameric sequence at genus, species, strain and serotype level [20].

## 4. Conclusions

The potential use of aptameric sequences as capture molecules for highly specific SERS detection of *E. coli* O157:H7 has been

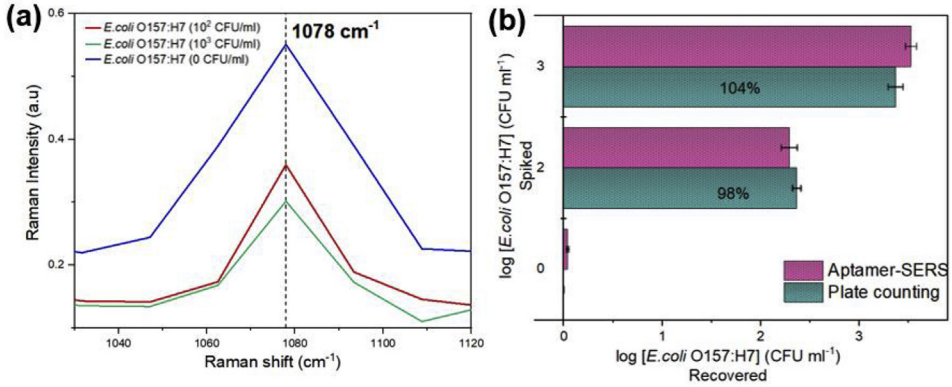


**Fig. 6.** Aptamer-based surface enhanced Raman scattering (SERS) detection of increasing concentrations (0–$10^3$ CFU/mL) of *E. coli* O157:H7 spiked in ground beef homogenized suspensions (a). Performance validation: aptamer-SERS detection vs. plate counting as a conventional testing method(b). All the results represent the average of 3 independent measurements.

**Table 1**
Recovery performance of Aptamer-SERS fabricated platform. Analysis of real samples spiked with E. *coli* O157:H7.

| Sample | Spiked concentration (CFU mL$^{-1}$) | Found concentration (CFU mL$^{-1}$) | | Recovery % | RSD % |
|---|---|---|---|---|---|
| | | SERS signal (1078 cm$^{-1}$) | Quantitative Analysis | | |
| Ground beef | 0 | 0.56 | 0.00 | NA | |
| Ground beef | $3.51 \times 10^2$ | 0.31 | $3.48 \times 10^2$ | 99.64 | 3.65 |
| Ground beef | $3.51 \times 10^3$ | 0.28 | $3.77 \times 10^3$ | 113.04 | 2.89 |

**Table 2**
Comparison of the Analytical SERS-based platforms reported for detection of *E. coli* O157:H7.

| Analytical method | Capture biomolecule | Sample tested and complexity (+) | LOD (CFU mL$^{-1}$) | Ref |
|---|---|---|---|---|
| Immunocapture- Ag/Au core-shell NPs | Antibody | Phosphate buffer (+) | 100 | [15] |
| Sandwich-Immunomagnetic separation | Monoclonal antibody | Filtered water (+) | 28 | [39] |
| Immunomagnetic capture-Silica encapsulated AuNPs | Monoclonal antibody | River water (++) | 10 | [40] |
| Immunomagnetic separation | Monoclonal antibody | Apple juice (++) | 100 | [41] |
| **Aptamer- bare AUNPs** | **DNA-Aptamer** | **Ground beef (+++)** | 100 | **This work** |

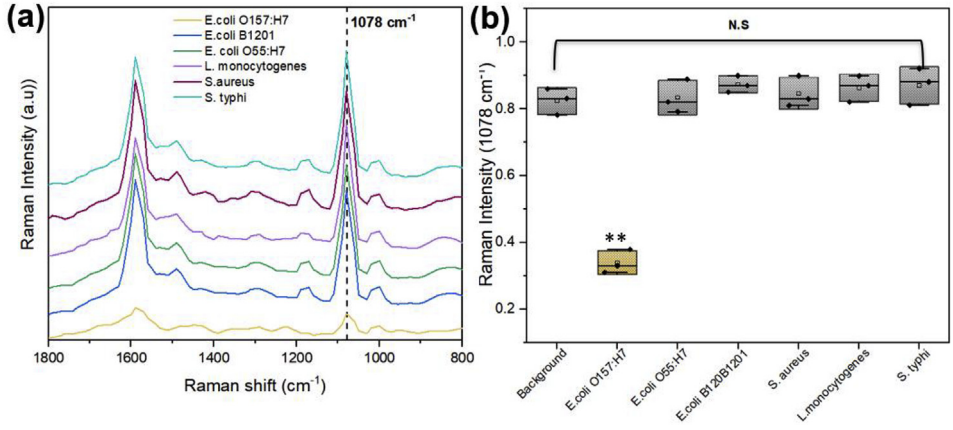


**Fig. 7.** Specificity Test: *E. coli* O157:H7 ($10^6$ CFU mL$^{-1}$) vs. interferent bacteria ($10^6$ CFU mL$^{-1}$). Control Sample: Phosphate Buffer Solution (pH 7,4) (0 CFU mL$^{-1}$) (a); Variation analysis and significance (means comparison) of Raman intensity response at 1078 cm$^{-1}$. Each result represents the average of 3 independent measurements; the area of the box represents 1SD, and the error bars 1.5 SD from the mean value (b).

demonstrated. In summary, we introduced the first aptamer-SERS platform for effective detection ($10^1$ CFU mL$^{-1}$) and quantification (LOD: $10^2$ CFU mL$^{-1}$) ($r^2 = 0.995$) of Shiga toxin producer *E. coli* O157:H7 in pure culture and ground beef homogenate. In addition, this work reveals the opportunity to overcome the limitations of conventional probes in respect to stability under harsh conditions, shelf-life, and signal variation from batch to batch. We showed that the proposed Raman probes possess a superior performance with high sensitivity and stability, compared with the conventional immune-based ones. To realize the practical implementation of the proposed detection platform, it would be necessary to carry out further evaluations under an extended set of experimental conditions, which could demonstrate its robustness. Knowing that one of the major factors controlling the dipolar localized surface plasmon resonance is the variation of the particle shape, future modifications of the particle shape and size may potentially be recommended. Then, the new reporter particles could be applied simultaneously to different foodborne pathogens in a multiplexed fashion and/or with strain-specific aptamer sequences.

## Declaration of interests

The authors declare that they have no known competing financial interests or personal relationships that could have appeared to influence the work reported in this paper.

## Acknowledgments

This material is based upon work supported by the U.S. Department of Agriculture, Agricultural Research Service, under Agreement ARS-CFSE funding No. 59-8072-6-001), project [No. 8072-42000-077-00D], and partially supported by COLCIENCIAS funding [756-2016]. Any opinions, findings, conclusion, or recommendations expressed in this publication are those of the author(s) and do not necessarily reflect the view of the U.S. Department of Agriculture.

## References

[1] S.E. Majowicz, E. Scallan, A. Jones-Bitton, J.M. Sargeant, J. Stapleton, F.J. Angulo, D.H. Yeung, M.D. Kirk, Global incidence of human Shiga toxin–producing Escherichia coli infections and deaths: a systematic review and knowledge synthesis, Foodborne Pathog. Dis. 11 (2014) 447–455, https://doi.org/10.1089/fpd.2013.1704.

[2] A.E. Tozzi, A. Caprioli, F. Minelli, A. Gianviti, L. De Petris, A. Edefonti, G. Montini, A. Ferretti, T. De Palo, M. Gaido, G. Rizzoni, Shiga Toxin–Producing Escherichia coli Infections Associated with Hemolytic Uremic Syndrome vol. 9, 2003, pp. 106–108. Italy, 1988–2000, Emerging Infectious Diseases, https://www.ncbi.nlm.nih.gov/pmc/articles/PMC2873761/pdf/02-0266.pdf. accessed May 9, 2018.

[3] S.M. Chekabab, J. Paquin-Veillette, C.M. Dozois, J. Harel, The ecological habitat and transmission of Escherichia coli O157:H7, FEMS (Fed. Eur. Microbiol. Soc.) Microbiol. Lett. 341 (2013) 1, https://doi.org/10.1111/1574-6968.12078.

[4] N. Pihkala, B. Nathan, D. Eblen, P. Evans, R. Johnson, J. Webb, C. Williams, Risk Profile for Pathogenic Non-o157 Shiga Toxin-Producing Escherichia coli (Non-o157 STEC), 2012. https://www.fsis.usda.gov/PDF/Non_O157_STEC_Risk_Profile_May2012.pdf.

[5] P.D. Frenzel, A. Drake, F.J. Angulo, Economic cost of illness due to Escherichia coli O157 infections in the United States, J. Food Prot. 68 (2005) 2623–2630, https://doi.org/10.4315/0362-028X-68.12.2623.

[6] A.K. Deisingh, M. Thompson, Strategies for the detection of Escherichia coli O157:H7 in foods, J. Appl. Microbiol. 96 (2004) 416–429, https://doi.org/10.1111/j.1365-2672.2003.02170.x.

[7] P.A. Chapman, Methods available for the detection of Escherichia coli O157 in clinical, food and environmental samples, World J. Microbiol. Biotechnol. 16 (2000) 733–740, https://doi.org/10.1023/a:1008985008240.

[8] J. Teng, F. Yuan, Y. Ye, L. Zheng, L. Yao, F. Xue, W. Chen, B. Li, Aptamer-based technologies in foodborne pathogen detection, Front. Microbiol. 7 (2016) 1–11, https://doi.org/10.3389/fmicb.2016.01426.

[9] A. Chen, S. Yang, Replacing antibodies with aptamers in lateral flow immunoassay, Biosens. Bioelectron. 71 (2015) 230–242, https://doi.org/10.1016/j.bios.2015.04.041.

[10] J.L. Holland, L. Louie, A.E. Simor, M. Louie, PCR detection of Escherichia coli O157:H7 directly from stools: evaluation of commercial extraction methods for purifying fecal DNA, J. Clin. Microbiol. 38 (2000) 4108–4113, 0095-1137/

00/$04.00+0.
[11] L.P. Godambe, J. Bandekar, R. Shashidhar, Species Specific PCR Based Detection of Escherichia coli from Indian Foods, vol. 3, 2017, pp. 2–5, https://doi.org/10.1007/s13205-017-0784-8. Biotech. 7.
[12] J. Chen, B. Park, Y. wen Huang, Y. Zhao, Y. Kwon, Label-free SERS detection of Salmonella Typhimurium on DNA aptamer modified AgNR substrates, J. Food Meas. Char. 11 (2017) 1773–1779, https://doi.org/10.1007/s11694-017-9558-6.
[13] Y. Liu, H. Zhou, Z. Hu, G. Yu, D. Yang, J. Zhao, Label and label-free based surface-enhanced Raman scattering for pathogen bacteria detection: a review, Biosens. Bioelectron. (2017), https://doi.org/10.1016/j.bios.2017.02.032.
[14] C.N. Kotanen, L. Martinez, R. Alvarez, J.W. Simecek, Surface enhanced Raman scattering spectroscopy for detection and identification of microbial pathogens isolated from human serum, Sens. Bio-Sens. Res. 8 (2016) 20–26, https://doi.org/10.1016/j.sbsr.2016.03.002.
[15] S.P. Ravindranath, Y. Wang, J. Irudayaraj, SERS driven cross-platform based multiplex pathogen detection, Sens. Actuators B Chem. 152 (2010) 183–190, https://doi.org/10.1016/j.snb.2010.12.005.
[16] I.-H. Cho, P. Bhandari, P. Patel, J. Irudayaraj, Membrane filter-assisted surface enhanced Raman spectroscopy for the rapid detection of E. coli O157:H7 in ground beef, Biosens. Bioelectron. 64 (2014) 171–176, https://doi.org/10.1016/j.bios.2014.08.063.
[17] T. Zhu, Y. Hu, K. Yang, N. Dong, M. Yu, N. Jiang, A novel SERS nanoprobe based on the use of core-shell nanoparticles with embedded reporter molecule to detect E. coli O157:H7 with high sensitivity, Microchimica Acta 185 (2018) 1–9, https://doi.org/10.1007/s00604-017-2573-9.
[18] E.C. Alocilja, S.M. Radke, Market analysis of biosensors for food safety, Biosens. Bioelectron. 18 (2003) 841–846, https://doi.org/10.1016/S0956-5663(03)00009-5.
[19] S. Diaz-Amaya, L.K. Lin, R.E. DiNino, C. Ostos, L.A. Stanciu, Inkjet printed electrochemical aptasensor for detection of Hg2+ in organic solvents, Electrochim. Acta 316 (2019) 33–42, https://doi.org/10.1016/j.electacta.2019.05.079.
[20] S. Díaz-Amaya, M. Zhao, L. Lin, C. Ostos, J.P. Allebach, G.T. Chiu, A.J. Deering, L.A. Stanciu, Inkjet Printed Nanopatterned Aptamer-Based Sensors for Improved Optical Detection of Foodborne Pathogens, Small. 1805342, 2019, pp. 1–14, https://doi.org/10.1002/smll.201805342.
[21] X. Yu, F. Chen, R. Wang, Y. Li, Whole-bacterium SELEX of DNA aptamers for rapid detection of E.coli O157:H7 using a QCM sensor, J. Biotechnol. 266 (2018) 39–49, https://doi.org/10.1016/j.jbiotec.2017.12.011.
[22] W. Wu, J. Zhang, M. Zheng, Y. Zhong, J. Yang, Y. Zhao, W. Wu, W. Ye, J. Wen, Q. Wang, J. Lu, An aptamer-based biosensor for colorimetric detection of Escherichia coli O157:H7, PLoS One 7 (2012) 1–9, https://doi.org/10.1371/journal.pone.0048999.
[23] W. Wu, S. Zhao, Y. Mao, Z. Fang, X. Lu, L. Zeng, A sensitive lateral flow biosensor for Escherichia coli O157:H7 detection based on aptamer mediated strand displacement amplification, Anal. Chim. Acta 861 (2015) 62–68, https://doi.org/10.1016/j.aca.2014.12.041.
[24] W. Gao, B. Li, R. Yao, Z. Li, X. Wang, X. Dong, H. Qu, Q. Li, N. Li, H. Chi, B. Zhou, Z. Xia, Intuitive label-free SERS detection of bacteria using aptamer-based in situ silver nanoparticles synthesis, Anal. Chem. (2017), https://doi.org/10.1021/acs.analchem.7b01813.
[25] H. Zhang, X. Ma, Y. Liu, N. Duan, S. Wu, Z. Wang, B. Xu, Gold nanoparticles enhanced SERS aptasensor for the simultaneous detection of Salmonella typhimurium and Staphylococcus aureus, Biosens. Bioelectron. 74 (2015) 872–877, https://doi.org/10.1016/j.bios.2015.07.033.
[26] C. Zhang, C. Wang, R. Xiao, L. Tang, J. Huang, D. Wu, S. Liu, Y. Wang, D. Zhang, S. Wang, X. Chen, Sensitive and specific detection of clinical bacteria: via vancomycin-modified Fe 3 O 4 @Au nanoparticles and aptamer-functionalized SERS tags, J. Mater. Chem. B 6 (2018) 3751–3761, https://doi.org/10.1039/c8tb00504d.
[27] A. Lehmacher, H. Meier, S. Aleksic, J. Bockemühl, Detection of hemolysin variants of Shiga toxin-producing Escherichia coli by PCR and culture on vancomycin-cefixime-cefsulodin blood agar, Appl. Environ. Microbiol. 64 (1998) 2449–2453.
[28] H. Schmidt, H. Karch, Enterohemolytic phenotypes and genotypes of Shiga toxin-producing Escherichia coli O111 strains from patients with diarrhea and hemolytic- uremic syndrome, J. Clin. Microbiol. 34 (1996) 2364–2367.
[29] H. Fleming, R. McFeeters, F. Breidt, Compendium of methods for the microbiological examination of foods, in: F. Pouch Downes, K. Ito (Eds.), Compendium of Methods for the Microbiological Examination of Foods, fourth ed., APHA Press, Washington DC, 2015, pp. 521–532.
[30] J.G. Bruno, J. Chanpong, Methods of Producing Competitive Aptamer FRET Reagents and Assays, 2009, US20090186342.
[31] J. Gao, X. Huang, H. Liu, F. Zan, J. Ren, Colloidal stability of gold nanoparticles modified with thiol compounds: bioconjugation and application in cancer cell imaging, Langmuir 28 (2012) 4464–4471, https://doi.org/10.1021/la204289k.
[32] A. Spasic, S.M. Assmann, P.C. Bevilacqua, D.H. Mathews, Modeling RNA secondary structure folding ensembles using SHAPE mapping data, Nucleic Acids Res. 46 (2018) 314–323, https://doi.org/10.1093/nar/gkx1057.
[33] F. Ricci, R.Y. Lai, A.J. Heeger, K.W. Plaxco, J.J. Sumner, Effect of molecular crowding on the response of an electrochemical DNA sensor, Langmuir 23 (2007) 6827–6834, https://doi.org/10.1021/la700328r.
[34] I. Muslum, M. Nilsen-Hamilton, Aptamers in analytics, Analyst 141 (2016) 1551–1568, https://doi.org/10.1039/c5an01824b.
[35] A. Dhiman, P. Kalra, V. Bansal, J.G. Bruno, T.K. Sharma, Aptamer-based point-of-care diagnostic platforms, Sens. Actuators B Chem. 246 (2017) 535–553, https://doi.org/10.1016/j.snb.2017.02.060.
[36] Y. Seok Kim, N.H. Ahmad Raston, M. Bock Gu, Aptamer-based nanobiosensors, Biosens. Bioelectron. 76 (2016) 2–19, https://doi.org/10.1016/j.bios.2015.06.040.
[37] J.G. Bruno, M.P. Carrillo, T. Phillips, C.J. Andrews, A novel screening method for competitive FRET-aptamers applied to E. coli assay development, J. Fluoresc. 20 (2010) 1211–1223, https://doi.org/10.1007/s10895-010-0670-9.
[38] J.G. Bruno, Evaluation of the ability of anti-lipopolysaccharide aptamers to discriminate various pathogenic, Aptamers Synth. Antib. 3 (2017) 55–63.
[39] B. Guven, N. Basaran-Akgul, E. Temur, U. Tamer, I.H. Boyaci, SERS-based sandwich immunoassay using antibody coated magnetic nanoparticles for Escherichia coli enumeration, Analyst 136 (2011) 740–748, https://doi.org/10.1039/c0an00473a.
[40] T. Zhu, Y. Hu, K. Yang, N. Dong, M. Yu, N. Jiang, A novel SERS nanoprobe based on the use of core-shell nanoparticles with embedded reporter molecule to detect E. coli O157:H7 with high sensitivity, Microchimica Acta 185 (2018) 1, https://doi.org/10.1007/s00604-017-2573-9.
[41] R. Najafi, S. Mukherjee, J. Hudson, A. Sharma, P. Banerjee, Development of a rapid capture-cum-detection method for Escherichia coli O157 from apple juice comprising nano-immunomagnetic separation in tandem with surface enhanced Raman scattering, Int. J. Food Microbiol. 189 (2014) 89–97, https://doi.org/10.1016/j.ijfoodmicro.2014.07.036.